IOPscience iopscience.iop.org

Home Search Collections Journals About Contact us My IOPscience

Electron spin relaxation of vibronic $Cu(H_2O)_6$ complexes in $K_2Zn(SO_4)_2 \cdot 6H_2O$ single crystals

This article has been downloaded from IOPscience. Please scroll down to see the full text article.

2001 J. Phys.: Condens. Matter 13 707

(http://iopscience.iop.org/0953-8984/13/4/316)

View the table of contents for this issue, or go to the journal homepage for more

Download details:
IP Address: 171.66.16.226
The article was downloaded on 16/05/2010 at 08:25

Please note that terms and conditions apply.

INSTITUTE OF PHYSICS PUBLISHING JOURNAL OF PHYSICS: CONDENSED MATTER

J. Phys.: Condens. Matter **13** (2001) 707–718 www.iop.org/Journals/cm PII: S0953-8984(01)14290-6

Electron spin relaxation of vibronic $Cu(H_2O)_6$ complexes in $K_2Zn(SO_4)_2{\cdot}6H_2O$ single crystals

S K Hoffmann[1], **J Goslar, W Hilczer and M A Augustyniak-Jabłokow**

Institute of Molecular Physics, Polish Academy of Sciences, Smoluchowskiego 17, PL-60179 Poznań, Poland

E-mail: skh@ifmpan.poznan.pl

Received 23 May 2000, in final form 16 November 2000

Abstract

The low temperature (6 K) EPR spectrum of Cu^{2+} in $K_2Zn(SO_4)_2{\cdot}6H_2O$ is characteristic for the ground state $a|x^2 - y^2\rangle - b|z^2\rangle$ with essentially the $|x^2 - y^2\rangle$ state and 4.5% admixture of the $|z^2\rangle$ state due to the zero-point motions. Temperature variations of the g and A parameters are characteristic for two-well vibronic dynamics and the vibronic averaging of the g-factor is well described with the simple Silver–Getz model above 60 K with energy difference $\delta_{12} = 68$ cm^{-1} between the wells. However, this model does not reproduce the $A(T)$ dependence, which seems to be influenced by temperature induced changes in the unpaired electron delocalization onto ligands. Electron spin relaxation was measured at low temperatures up to 55 K where the electron spin echo signal was detectable. At low temperatures, in the static Jahn–Teller limit, the $Cu(H_2O)_6$ complexes are strongly localized in the deepest potential well and the slow vibronic dynamics is overdominated by two-phonon Raman processes in electron spin–lattice relaxation. The relaxation rate is described by $1/T_1 = aT^9 I_8(\Theta_D/T)$ with transport integral I_8 and the Debye temperature $\Theta_D = 170$ K. Electron spin echo decay is strongly modulated by dipolar coupling with ^{1}H and ^{39}K nuclei and the decay function is $V(2\tau) = V_0 \exp(-a\tau - m\tau^2)$. The quadratic term dominates in the static Jahn–Teller limit (below 18 K) and describes the decay produced by the nuclear spectral diffusion. For higher temperatures the $\exp(-a\tau)$ term dominates and describes an effect of the intrawell excitations with phase relaxation rate $1/T_M = a + b\exp(-\Delta/kT)$ with $\Delta = 67$ cm^{-1} being the energy of the first excited vibronic level. The excitations produce a clear broadening of the Fourier transform electron spin echo (FT-ESE) spectra (at 18 K), where peaks from potassium and hydrogen nuclei have been identified.

1. Introduction

Diamagnetic Tutton salt type crystals $M^I_2M^{II}(SO_4)_2{\cdot}6H_2O$ contain hexaaqua complexes of the divalent M^{II} cations (M^{II} = Zn, Cd, Mg, ...) with a weakly disturbed octahedral

[1] Author to whom correspondence should be addressed.

0953-8984/01/040707+12$30.00 © 2001 IOP Publishing Ltd Printed in the UK

geometry, due to the hydrogen bonds with surrounding SO_4^{2-} groups. In paramagnetic crystals with $M^{II} = Cu^{2+}$ a strong deformation of the octahedra appears as a result of the Jahn–Teller effect, as well as cooperative elastic couplings between vibronic octahedra [1–5]. The strong Jahn–Teller effect with the stabilization energy higher than the vibronic energy appears also in Cu^{2+}-doped diamagnetic Tutton salts [6–9]. Despite the very similar molecular and crystal structure, the vibrational effects observed by EPR spectroscopy in various diamagnetic $M_2^I M^{II}(SO_4)_2{\cdot}6H_2O{:}Cu^{2+}$ crystals are not so similar one to another as could be expected. This seems to be related to small differences in details of the adiabatic potential surface and hydrogen bond network. The characteristic feature of $Cu(H_2O)_6^{2+}$ vibrational complexes in Tutton salt type crystals is a relatively large difference δ in energy between Jahn–Teller distorted octahedral configurations. This difference is comparable to the energy $\hbar\omega$ of the first excited vibronic level.

Electron spin–lattice relaxation is expected to be governed by Jahn–Teller vibronic dynamics, i.e. thermally activated reorientations of the $Cu(H_2O)_6$ octahedron between the three distorted configurations, with a characteristic temperature dependence of the spin–lattice relaxation rate at low temperatures [10, 11]:

$$\frac{1}{T_1} = aT^3 + bT^5. \tag{1}$$

However, the literature data for various systems [12, 13] show that such behaviour is hardly ever observed, since the relaxation is dominated by the ordinary two-phonon Raman processes or Orbach–Aminov processes. Which of these contributions dominates depends on δ, barrier height, vibrational coupling coefficients and energy of the vibronic levels. The situation is, however, far from being clear and understood, both from theoretical and experimental points of view, especially for electron spin–spin relaxation (phase relaxation).

We have studied electron spin relaxation of Cu^{2+} in $(NH_4)_2Mg(SO_4)_2{\cdot}6H_2O$ crystals [12, 14] and found out that the Raman processes are responsible for relaxation up to 100 K. The vibronic g-factor averaging in the crystal varies with temperature in a distinctly different way as compared to other Tutton salt crystals, and cannot be well described either by Silver–Getz [6] or Riley–Hitchman [8] models widely used to describe $g(T)$ vibronic effects. Thus, we have decided to measure the electron spin relaxation of Cu^{2+} in the $K_2Zn(SO_4)_2{\cdot}6H_2O$ crystal, which is believed to exhibit a 'model' vibronic behaviour among Tutton salt crystals [6]. The hydrogen bond network is less dense in this crystal compared to $(NH_4)_2Mg(SO_4)_2{\cdot}6H_2O$, and the Jahn–Teller induced deformation of $Cu(H_2O)_6$ octahedra is the smallest among the Tutton salt crystals with energy difference between the two lowest potential energy wells $\delta_{12} = 68\ cm^{-1}$ [9] or $\delta_{12} = 75\ cm^{-1}$ [6]. Thus, one can expect that the transition rate between two potential wells will be higher as compared to $(NH_4)_2Mg(SO_4)_2{\cdot}6H_2O$, where $\delta_{12} = 108\ cm^{-1}$ [14] and the influence of Jahn–Teller dynamics on spin relaxation rate can be recognized. As well as for the spin–lattice relaxation we have studied the electron phase relaxation and ESEEM (electron spin echo envelope modulation) spectra, which seem to be more sensitive to molecular dynamics.

2. Experiment

$K_2Zn(SO_4)_2{\cdot}6H_2O$ crystals grow easily from saturated water solution. Crystals are monoclinic with $P2_1/a$ ($Z = 2$) and unit cell dimensions $a = 0.9034$ nm, $b = 1.2184$ nm, $c = 0.6148$ nm and $\beta = 104.8^\circ$ [15]. The crystals were doped with ^{63}Cu isotope by adding $^{63}CuSO_4{\cdot}5H_2O$ to the mother solution with resulting Cu^{2+} concentration 7×10^{17} spins g^{-1}. EPR and electron spin echo (ESE) measurements were performed on a Bruker ESP380E FT/CW spectrometer

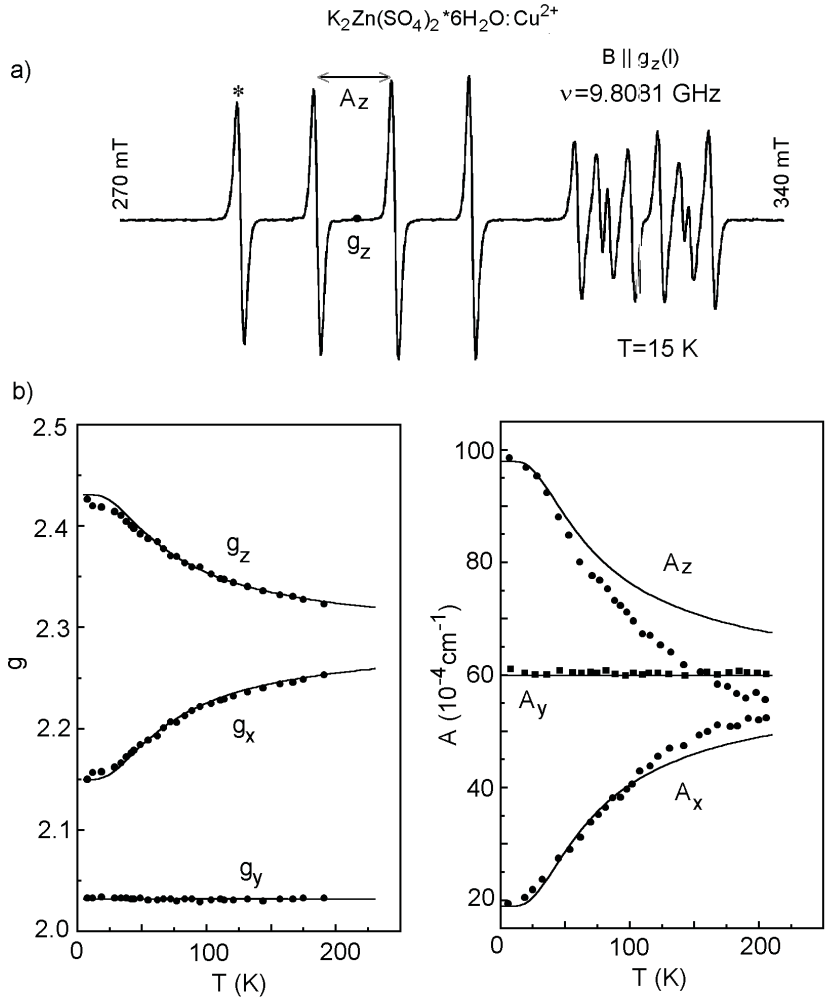

Figure 1. (a) EPR spectrum of Cu^{2+} ions recorded along the g_z-direction of the $Cu(H_2O)_6$ complex (I) at 15 K. The high-field lines centred around 330 mT are the allowed and forbidden hyperfine transitions in perpendicular orientation of the complex (II) magnetically inequivalent with (I) (see [14] for details). The asterisk marks the line for which the pulsed EPR experiments were performed. (b) Temperature variations of the principal g and A tensor components. The solid curves present the theoretical plots according to the two-well jump model with $\delta_{12} = 68\ \mathrm{cm}^{-1}$.

equipped with an Oxford CF935 flow helium cryostat. The temperature dependence of the g-factor and hyperfine splitting A was determined along the local crystal field symmetry axes, being Cu–O directions of $Cu(H_2O)_6$ octahedra.

Electron spin relaxation was measured along the g_z-axis direction, where hyperfine lines are well separated, and a 16 ns microwave pulse with spectral width of 2.2 mT exciting the whole $m_I = -3/2$ line. The EPR spectrum observed in this crystal orientation is shown in figure 1(a) and the excited line is marked by an asterisk.

Owing to the low Cu^{2+} concentration we have not observed effects either from electron spectral diffusion or instantaneous diffusion.

The spin–lattice relaxation time T_1 was determined using the saturation recovery method with a 24 ns saturation pulse, which allowed us to obtain the full saturation observed as a vanishing of the ESE signal. The recovery of the magnetization was single exponential in the whole temperature range, and was monitored by the amplitude of a Hahn-type ESE signal generated by two 16 ns pulses separated by 144 ns. The phase memory time T_M describing the dephasing of the spin precessional motion was measured with the same two-pulse sequence. The ESE decay was strongly modulated by weak interactions with surrounding hydrogen and potassium nuclei.

3. Results and discussion

3.1. Cw-EPR and vibronic averaging of the g and A parameters

Copper(II) ions introduced into the $K_2Zn(SO_4)_2{\cdot}6H_2O$ crystal substitute for Zn(II) ions located in the centre of the weakly deformed $Zn(H_2O)_6$ octahedra. Due to the Jahn–Teller effect the Cu^{2+} ions produce a strong deformation of the host octahedra. At low temperatures the Jahn–Teller effect is the static type and all $Cu(H_2O)_6$ complexes are localized in the deepest potential well of the adiabatic potential surface, i.e. are elongated along the same local O–Cu–O axis (z-axis). In this rigid lattice limit the EPR parameters determined from rotational data at 6 K are

$$g_x = 2.150(2) \qquad g_y = 2.032(2) \qquad g_z = 2.431(1)$$
$$A_x = -19(1) \qquad A_y = +60(1) \qquad A_z = -98(1) \times 10^{-4}\ \mathrm{cm}^{-1}$$

and are close, but with higher accuracy, to the literature data [7, 16]. Moreover, in the previous papers, except for [17], the signs of the hyperfine splitting parameters A_i and the g_x to g_y relation have not been derived and discussed. Because $g_y < 2.04$, the ground orbital state $|x^2 - y^2\rangle$ of Cu^{2+} has an admixture of the excited $|z^2\rangle$. Thus the ground state wavefunction has the form:

$$|0\rangle = \alpha[a|x^2 - y^2\rangle - b|z^2\rangle] \qquad a^2 + b^2 = 1$$

where α is the orbital reduction factor, and the mixing is produced by zero-point motions in the ground vibrational state. Following the McGarvey approach [18] and using the fitting procedure described in detail in [19], we found the electronic structure parameters α^2, a, b, Fermi contact hyperfine constant κ and orbital level energies E_{ij}, as summarized in table 1. The procedure gives the signs of the A_i-parameters and indicates that the 4.5% admixture of the $|z^2\rangle$ into $|x^2 - y^2\rangle$ produces $g_x > g_y$ with a significant g-tensor nonaxiality and $g_y < 2.04$ (see discussion in [19]). The calculated orbital energies fit well with optical d–d band positions, which for distorted $Cu(H_2O)_6$ octahedra are in the range 10 000–14 000 cm^{-1} [20, 21].

When temperature increases, the dynamic Jahn–Teller effect appears as the excitations of the $Cu(H_2O)_6$ to the higher energy vibronic levels and jumps to the other Jahn–Teller distorted configurations (higher energy potential wells corresponding to the octahedron elongations along Cu–ligand directions). The jumps and rapid back-relaxation produce a mixing of the configurations resulting in averaging of the EPR spin-Hamiltonian parameters g_i and A_i.

Table 1. Electronic structure parameters for Cu(II) complexes in $K_2Zn(SO_4)_2{\cdot}6H_2O$. Orbital energies E_{ij} are in (cm^{-1}) $\pm$ 80.

a	b	α^2	κ	E_{xy}	E_{xz}	E_{yz}
0.977(1)	0.213(1)	0.912(4)	0.256(2)	13 590	18 690	17640

Such averaging starting from the lowest temperatures is shown for g-factors and hyperfine splittings in figure 1(b). Since the g_y and A_y are temperature independent the higher energy well is not populated up to 200 K. This means that the shortest Cu–O bond in $Cu(H_2O)_6$ octahedra is not involved in vibronic dynamics. Thus, one can use the asymmetrical two-well model for description of the vibronic averaging effects [6, 8]. The model is widely used in description of the vibronic g-factor averaging for Cu^{2+} ions in various crystals. It is believed that the model is a very good approximation for Cu^{2+} in $K_2Zn(SO)_4{\cdot}6H_2O$, but a much worse one in other Tutton salt crystals. It must be stressed, however, that according to the results of [6, 9], the two-well model is not valid for $K_2Zn(SO)_4{\cdot}6H_2O$ below 40 K, where complexes are localized in the deepest potential well. Recently, we have discussed this problem on the basis of Cu^{2+} measurements in $(NH_4)_2Mg(SO_4)_2{\cdot}6H_2O$, where deviations from predictions of the two-well model are most pronounced [14]. Our $g(T)$ results can be fitted with the model above 60 K using $\delta_{12} = 68(2)\ \mathrm{cm}^{-1}$ as the energy difference between the wells, whereas in [6] $\delta_{12} = 75\ \mathrm{cm}^{-1}$ was found. The fitting is shown as a full curve in figure 1(b).

In all papers dealing with vibronic averaging effects in EPR spectra of Cu^{2+} ions only the g-factor averaging is discussed. However, the hyperfine splitting is also averaged and its temperature variations are measurable with even higher accuracy. Our data are shown in figure 1(b), and the fitting, with the same model and δ_{12}, is shown as the full curves. It is clearly seen that almost full averaging of hyperfine splitting appears at about 200 K, which is not predicted by the model. Moreover, the average value $(A_z + A_x)/2$ decreases with temperature in contrast to the $(g_z + g_x)/2$. This means that the isotropic hyperfine constant decreases on heating. This indicates that the electronic structure of $Cu(H_2O)_6$ complexes is affected by temperature, with higher delocalization of the unpaired electron density onto the ligand at higher temperatures.

3.2. Electron spin–lattice relaxation

It is generally assumed that vibronic dynamics can be a very effective mechanism of electron spin–lattice relaxation, leading to a transfer of the excitation energy of a spin system to the crystal lattice vibrations. The primary mechanism is related to thermally activated transitions between Jahn–Teller distorted configurations via tunnelling from the ground and excited vibronic levels. The reorientations over and through the potential barrier between adjacent potential wells as well as the phonon-controlled and phonon-assisted tunnelling have been already treated by quantum mechanical theory [22, 23]. The theory allows us to calculate the reorientation relaxation time τ describing the recovery of the thermal equilibrium between populations of the distorted configurations. The spin–lattice relaxation rate $1/T_1$ is, however, slower than the reorientation rate $1/\tau$, since only reorientations with simultaneous spin-flips are involved in the magnetic relaxation. The spin-flips are allowed because of the difference in anisotropy of the g-factor and hyperfine splitting for the different configurations [11]. Such a mechanism predicts a large anisotropy of T_1 in single crystals, which has never been observed. There exists, however, a possibility that both rates are identical when spin–orbit phonon-controlled tunnelling operates between the configurations [24, 25].

Another process which can produce spin–lattice relaxation is the Orbach–Aminov process involving excitations to the high energy level Δ. In Jahn–Teller systems this level can be the excited vibronic level, having mixed vibrational and electronic states in contradiction to other systems where the relaxation via excited pure vibrational level is not possible. Thus, generally the contributions to the spin–lattice relaxation rate in Jahn–Teller systems can be written as

$$\frac{1}{T_1} = aT + bT^3 I_2 + cT^5 I_4 + d\exp(-\Delta/kT) + fT^9 I_8 \qquad (2)$$

where I_n are the appropriate transport integrals over the Debye-type phonon spectrum

$$I_n(\Theta_D/T) = \int_0^{\Theta_D/T} \frac{x^n \exp(x)}{[\exp(x)-1]^2}\,\mathrm{d}x$$

where Θ_D is the Debye temperature. The aT term describes direct one-phonon relaxation process. The bT^3 term describes relaxation in the static Jahn–Teller limit, where vibronic reorientations are due to the tunnelling between equivalent potential wells, with b-coefficient depending on $(3\Gamma)^2$, where 3Γ is the splitting of the ground vibronic state [10]. The cT^5 term describes the dynamic Jahn–Teller effect due to the phonon-controlled tunnelling via excited vibronic states of energy Δ and/or phonon-assisted tunnelling via virtual phonon states [10]. The c-coefficient depends on the Δ and δ_{12}. The exponential term describes the Orbach–Aminov process with coefficient d depending on Δ^3. The last term fT^9 describes two-phonon Raman processes via the Van Vleck mechanism, which is a leading term in ionic crystals. The T^3 and T^5 terms can dominate in T_1-relaxation when potential wells are equivalent or nearly equivalent as for Cu^{2+} in $ZnSiF_6{\cdot}6H_2O$ [26]. The exponential type T_1-relaxation was found in $Zn(BrO_3)_2{\cdot}6H_2O{:}Cu^{2+}$ [27] and for Cu^{2+} in SrF_2 crystal [13] having small differences in energy between adjacent wells. In Tutton salt crystals the inequivalence δ_{12} in energy between potential wells is large, being of the order of the vibronic level splitting Δ. Thus, the T^3, T^5 and $\exp(-\Delta/kT)$ type relaxation can be overdominated by ordinary phonon processes. In fact, in $(NH_4)_2Mg(SO_4)_2{\cdot}6H_2O$ crystals doped with Cu^{2+} or Mn^{2+} ions we found [12] that the spin relaxation is governed by the Raman processes described by the fT^9 term. The results of temperature measurement of $1/T_1$ for Cu^{2+} in the $K_2Zn(SO_4)_2{\cdot}6H_2O$ crystal are shown in figure 2. The results were collected up to 50 K only, since the electron spin echo signal was not detectable at higher temperatures. The magnetization recovery was single exponential in the whole temperature range, as shown in the inset in figure 2 for 15 K. This indicates that the distribution of the doped Cu^{2+} ions is uniform in the crystal. The $1/T_1$ dependence was well

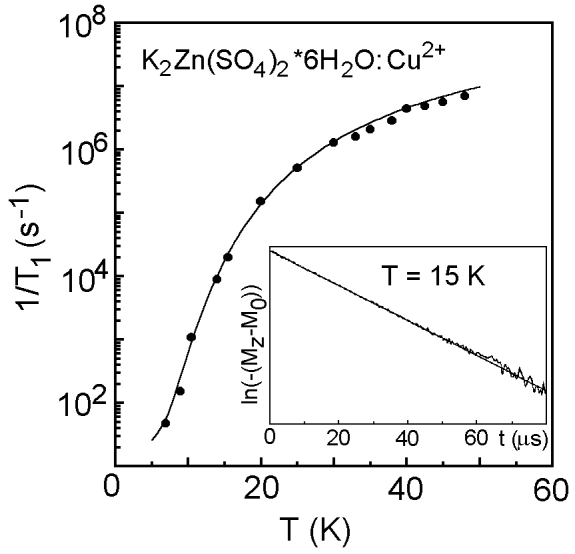

Figure 2. Temperature dependence of the spin–lattice relaxation rate. The solid curve is a plot of the equation $T_1^{-1} = 1.44 \times 10^{-11} T^9 I_8(170/T)$. The inset shows the recovery of the magnetization at 15 K.

fitted with the equation:

$$1/T_1 = fT^9 I_8(\Theta_D/T)$$

with $f = 1.44 \times 10^{-11}$ s^{-1} K^{-9} and the Debye temperature $\Theta_D = 170(5)$ K. The best fit is shown as a solid line in figure 2. The results show that up to 50 K the spin–lattice relaxation is dominated by two-phonon processes and the Debye temperature is slightly lower than for the Mg Tutton salt where we found $\Theta_D = 240(5)$ K.

3.3. Electron phase relaxation

For a small concentration of paramagnetic centres the electron spectral diffusion and instantaneous diffusion effects are negligible. In such a case, in the rigid lattice limit, the dephasing of the electron precessional motion is due to the nuclear spectral diffusion, i.e. fluctuations of the local magnetic field produced by nuclear spin flip-flops. This is the situation in our crystal. In such a case the theory of the ESE decay [28, 29] predicts that the ESE amplitude V varies with time τ (2τ is the interval between exciting and refocusing pulses):

$$V(2\tau) = V_0 \exp(-m\tau^k) \tag{3}$$

where $k \approx 2$ for long τ. The decay function can be described by the characteristic time T_M, which is called the phase memory time. The T_M is well defined for the exponential decay function with the linear power coefficient

$$V(2\tau) = V_0 \exp(2\tau/T_M) \tag{4}$$

but in the general case of exponential decay as in equation (3), the effective T_M can be defined as:

$$T_M = \left(\frac{1}{m}\right)^{1/k}. \tag{5}$$

The ESE decay observed for Cu^{2+} in $K_2Zn(SO_4)_2{\cdot}6H_2O$ is strongly modulated by weak dipolar coupling to surrounding ^{1}H ($I = 1/2$) and ^{39}K ($I = 3/2$) nuclei as shown in figure 3 for 8 K. In the case of strongly modulated ESE decay the separation of the modulation and decay functions into $V(2\tau) = V_{mod}V_{decay}$ is not a trivial task. In most cases the plot through the peaks of the $V(2\tau)$ function is used as a good approximation of the decay function. This does not allow us, however, to distinguish clearly between decay functions with different power coefficients k (equation (3)) (k can vary in the range 0.5–3). We propose to fit a decay function to the peaks in the $\log(V)$–τ^k scale. Such plots are shown in figures 3(b) and (c). It is clearly seen that the proper decay function is the quadratic type ($k = 2$) giving a linear plot in the logarithmic scale. This function with effective $T_M = 3.72$ μs is plotted as the solid curve in the experimental $V(2\tau)$–2τ dependence in figure 3(a). We found the quadratic type decay in the temperature range below 18 K. For higher temperatures the decay functions were clearly of linear type (equation (4)) with $k = 1$ and relaxation rate $1/T_M$ increasing progressively on heating. The resulting $1/T_M$–T plot is shown in a logarithmic scale in figure 4.

The acceleration of the phase relaxation on heating reflects a broadening of the spin packets, forming an inhomogeneously broadened EPR line, due to paramagnetic centre motions. The spin packet width can be evaluated as $1/T_M$, being 9.5 μT at 8 K and 16 μT at 55 K. An increase in the relaxation rate can be fitted with the following equation:

$$\frac{1}{T_M} = a + b\exp\left(-\frac{\Delta}{kT}\right) \tag{6}$$

and the fit is shown as a solid curve in figure 4 (the two term contributions are shown by dashed lines). The fitting parameters are: $a = 2.7 \times 10^5$ s^{-1}, giving $T_M^{rigid} = 3.7$ μs,

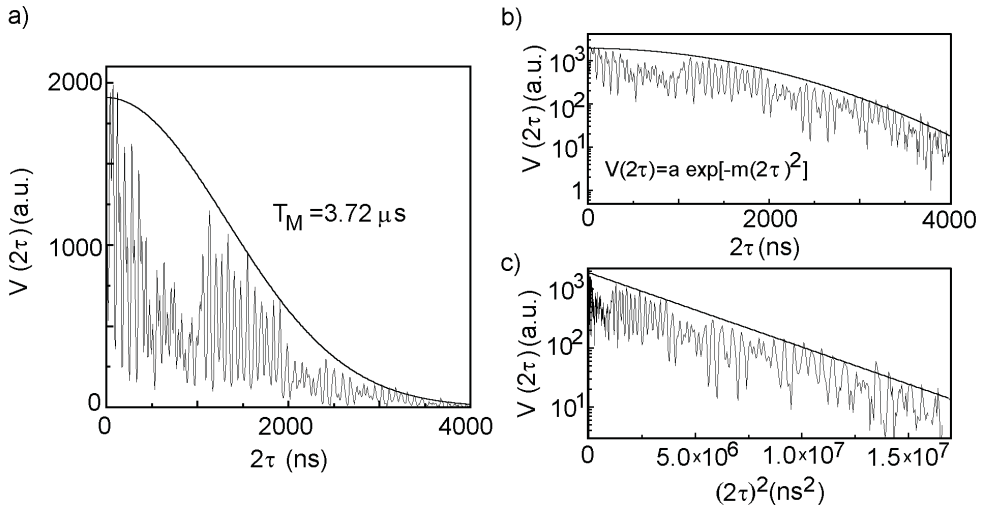

Figure 3. Electron spin echo decay at 8 K. (a) Experimental decay; (b) decay in log V against 2τ; (c) decay in log V against $(2\tau)^2$. The best fit with $V(2\tau) = a\exp[-m\tau^2]$ and $T_M = 3.72$ μs is shown as solid curves.

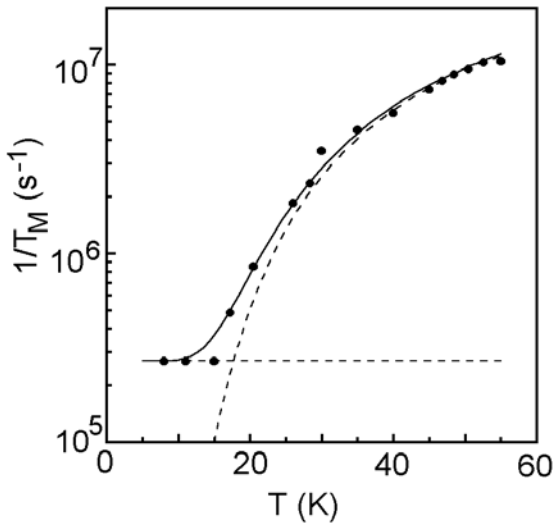

Figure 4. Temperature variations of the phase relaxation rate. The solid line is the best fit to relaxation equation $1/T_M = 0.27\times10^6 + 6.5\times10^7\exp(-\Delta/kT)$ with $\Delta = 67\,\mathrm{cm}^{-1}$. The dashed lines represent the temperature independent and exponential term.

$b = 6.5\times10^7$ s^{-1} and $\Delta = 67(3)$ cm^{-1} $= 97$ K. According to our results for $(NH_4)_2Mg(SO_4)_2{\cdot}6H_2O{:}Cu^{2+}$ [12, 14] the energy Δ can be assumed as the splitting between ground and excited vibronic levels in the deepest potential well. Thus, we assume that vibronic excitations and decay produce dephasing of the precessional motion decreasing ESE amplitude below 60 K where Jahn–Teller dynamics is still very slow.

Our experimental data allowed us to determine the energy difference δ_{12} between the two deepest energy wells (from vibronic g-factor averaging) and the energy Δ of the excited

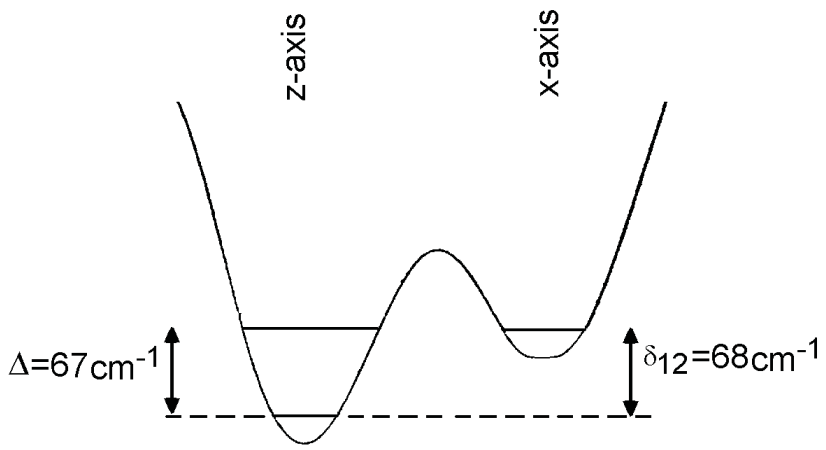

Figure 5. The two vibronic active potential energy wells with energy levels determined from cw-EPR and ESE results.

Table 2. Energy difference δ_{12} between two potential wells and excited vibronic level energy Δ (in cm^{-1}) for $Cu(H_2O)_6$ in Tutton salt crystals.

Crystal	δ_{12}	Δ	Reference
$K_2Zn(SO_4)_2{\cdot}6H_2O$	68(3)	67(3)	This paper
	75	120	[6]
$Cs_2Zn(SO_4)_2{\cdot}6H_2O$	318	71[a]	[32]
$(NH_4)_2Mg(SO_4)_2{\cdot}6H_2O$	108	102	[14]

[a] Our unpublished data.

vibronic state in the lowest energy well as shown in figure 5. These parameters for various Tutton salt crystals are shown in table 2. A peculiarity of $Cu(H_2O)_6$ in the $K_2Zn(SO_4)_2{\cdot}6H_2O$ crystal is that both energies δ_{12} and Δ are small and comparable in magnitude. Thus, a very effective tunnelling between the excited vibronic state of the z-well and the ground state of the x-well can operate at higher temperatures. For this reason the crystal exhibits vibronic properties which are closest to the assumptions of the two-well models among the Tutton salt crystals.

3.4. Electron spin echo envelope modulation (ESEEM) spectroscopy

The Fourier transform of the two-pulse ESE amplitude modulation function gives a pseudo-ENDOR spectrum containing peaks at main and combination nuclear frequencies. These peaks are due to a weak dipolar coupling between unpaired electron and magnetic nuclei lying at the distance in the range 0.25–0.5 nm. This area, restricted by two circles, is shown in the crystal structure of $K_2Zn(SO)_4{\cdot}6H_2O$ presented in figure 6. Thus, we can expect modulations and peaks in FT-ESE spectra from protons ^1H of the coordinated water molecules, as well as from the nearest potassium ^{39}K atoms. The spectra at 15 K and 20 K are shown in figure 7. Low frequency peaks origin from ^{39}K nuclear transitions (around 0.6 MHz) and its overtones. The peaks around 12.2 MHz and 24.5 MHz are at proton ^1H Larmor frequency ω_L and $2\omega_L$, respectively.

Among peaks around free proton frequency ω_L the doublets can be distinguished as marked in figure 7(a). The spectra were obtained with external magnetic field along the z-axis of the

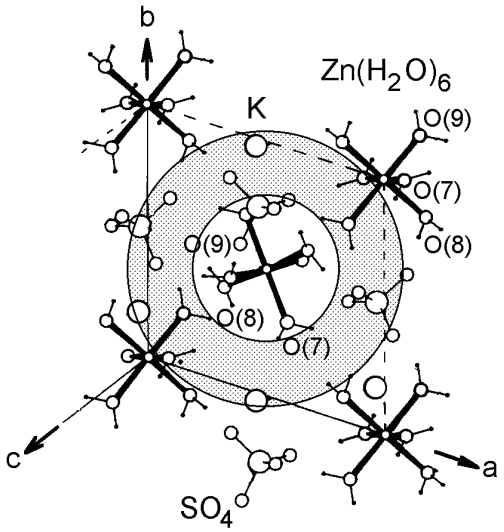

Figure 6. Projection of the $K_2Zn(SO_4)_2{\cdot}6H_2O$ structure along the [112] direction. Magnetic nuclei located in the area between two circles are expected to contribute to the ESEEM.

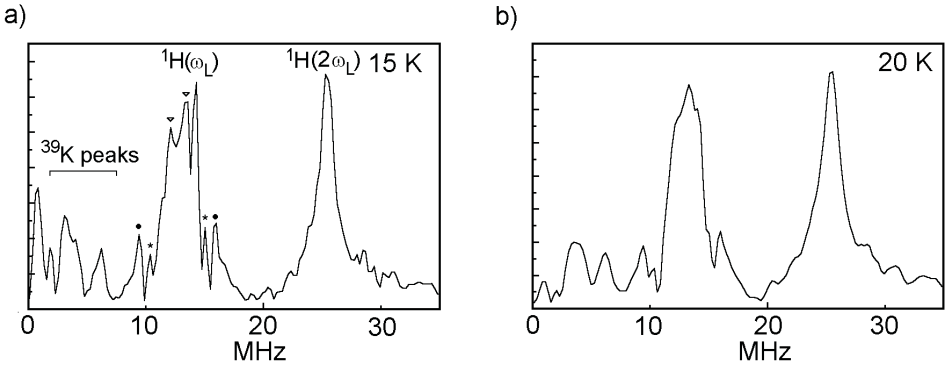

Figure 7. The Fourier transform of the modulation function (FT-ESE spectrum) recorded at 15 K and 20 K. The peaks assigned for ^{39}K and ^{1}H are marked with three doublets around the ω_L(^{1}H) frequency (see text).

$Cu(H_2O)_6$ complex. Thus, the two doublets with splittings 6.3 MHz and 4.8 MHz can be assigned as due to interactions with protons of water molecules coordinated at apical positions (z-axis), whereas the doublet with splitting 1.5 MHz can be due to interactions with in-plane water protons. The FT-ESE spectrum pattern is not affected by temperature up to about 18 K. At this temperature a rapid broadening of the lines appears, which smears out the observed structures (figure 7(b)) without noticeable change in the peak positions. This effect appears at the same temperature where the vibronic acceleration of the phase relaxation starts, and seems to have the same origin. We can conclude that ESE decay is sensitive to the vibronic dynamics. We have observed similar effects for Cu^{2+} in $(NH_4)_2Mg(SO_4)_2{\cdot}6H_2O$, where the modulation pattern was dominated by interactions with the nearest NH_4 groups and thermally activated reorientations of these groups produced broadening and averaging of proton peaks in the FT-ESE spectrum at about 60 K [30].

4. Conclusions

A characteristic property of $Cu(H_2O)_6$ in $K_2Zn(SO_4)_2{\cdot}6H_2O$ is that the energy difference $\delta_{12} = 68\,cm^{-1}$ between the two lowest energy potential wells (determined from EPR g-factors) is practically the same as the energy $\Delta = 67\,cm^{-1}$ of the first excited vibronic level (determined from electron phase relaxation). This warrants a higher effectivity of the tunnelling via the excited state to the higher energy well, which is not the case for other Tutton salt crystals.

The $K_2Zn(SO_4)_2{\cdot}6H_2O{:}Cu^{2+}$ is believed to be a 'model' system for description of the vibronic dynamics of $Cu(H_2O)_6$ complexes. Our data and an inspection of the previous papers show, however, that such a description is adequate for $T > 60$ K only. This means that the thermal equilibrium between two Jahn–Teller distorted configurations observed by the g-factor vibronic averaging is kept at a higher temperature range only. At lower temperatures the population ratio of the two configurations cannot be described by the Boltzmann statistics in the two-state model. There is no clear explanation of this effect.

At low temperatures the vibronic $Cu(H_2O)_6$ complexes are well localized in the deepest potential well and interwell jumps are relatively rare. For this reason the vibronic dynamics is not a very effective mechanism of spin–lattice relaxation, which is dominated by the ordinary two-phonon Raman processes. The relaxation rate is typical for Cu^{2+} complexes in contradiction to the claim of some rather old papers [26, 31]. This slow vibronic dynamics related to the dynamic Jahn–Teller effect gives clear effects in EPR spectra as an onset of the g-factor and hyperfine splitting averaging. On the other hand, the intrawell vibronic dynamics, i.e. excitations to the higher energy vibronic levels, is the effective mechanism of the electron precession dephasing, producing an acceleration of the phase relaxation rate $1/T_M$ above 18 K and rapid broadening of the FT-ESE spectra.

Acknowledgment

This work was supported by the Polish Scientific Research Committee under grant KBN-2-P03B-122-14.

References

[1] Simmons C J, Hitchman M A, Stratemeier H and Shultz A J 1993 *J. Am. Chem. Soc.* **115** 11 304
[2] Rauw W, Ahsbahs H, Hitchman M A, Lukin S, Reinen D, Schultz A J, Simmons C J and Stratemeier H 1996 *Inorg. Chem.* **35** 1902
[3] Hoffmann S K and Gomółka-Marciniak M 1993 *Solid State Commun.* **86** 63
[4] Hoffmann S K and Gomółka-Marciniak M 1993 *Acta Phys. Polon.* A **83** 817
[5] Marciniak M, Hoffmann S K, Augustyniak M A and Hilczer W 1995 *Phys. Status Solidi* b **191** 201
[6] Silver B L and Getz D 1974 *J. Chem. Phys.* **61** 638
[7] Petrashen V E, Yablokov Yu V and Davidovich R L 1980 *Phys. Status Solidi* b **101** 117
[8] Riley M J, Hitchman M A and Mohammed A W 1987 *J. Chem. Phys.* **87** 3766
[9] Augustyniak M A and Usachev A E 1999 *J. Phys.: Condens. Matter* **11** 4391
[10] Breen D P, Krupka D C and Williams F I B 1969 *Phys. Rev.* **179** 241
[11] Ham F S 1972 *Electron Paramagnetic Resonance* ed S Geschwind (New York: Plenum) ch 1
[12] Hoffmann S K, Augustyniak M A, Goslar J and Hilczer W 1998 *Mol. Phys.* **95** 1265
[13] Hoffmann S K and Ulanov V A 2000 *J. Phys.: Condens. Matter* **12** 1855
[14] Hoffmann S K, Goslar J, Hilczer W, Augustyniak M A and Marciniak M 1998 *J. Phys. Chem.* A **102** 1697
[15] Whitnall J, Kennard C H L, Nimmo K K and Moore F H 1975 *Cryst. Struct. Commun.* **4** 717
[16] Getz D and Silver B L 1974 *J. Chem. Phys.* **61** 630
[17] Rao T B and Narayana M 1981 *Phys. Status Solidi* b **106** 601
[18] McGarvey B R 1966 *Transition Metal Chemistry* ed R L Carlin (New York: Dekker) p 160
[19] Hoffmann S K, Goslar J and Szczepaniak L S 1986 *Phys. Status Solidi* b **133** 321

[20] Hitchman M A and Waite T D 1976 *Inorg. Chem.* **15** 2150
[21] Satyanarayana N and Radhakrishna S 1985 *Solid State Commun.* **54** 891
[22] Sussmann J A 1967 *J. Phys. Chem. Solids* **28** 1643
[23] Vikhnin V S 1978 *Fiz. Tverd. Tela* **20** 1340
[24] Bill H and Silbee R H 1974 *Phys. Rev.* B **10** 2697
[25] Zaritskii I M, Bratus V Ya, Vikhnin V S, Vishevskii A S, Kothits A A and Ustintsev V M 1976 *Fiz. Tverd. Tela* **18** 3226
[26] Dang L S, Buisson R and Williams F I B 1974 *J. Physique* **35** 49
[27] Jesion A, Shing Y H and Walsh D 1977 *Phys. Rev.* B **16** 3012
[28] Salikhov K M, Semenov A G and Tsvetkov Yu D 1976 *Electron Spin Echoes and Their Applications* (Novosibirsk: Science) ch 3
[29] Salikhov K M and Tsvetkov Yu D 1979 *Time Domain Electron Spin Resonance* ed L Kevan and R N Schwartz (New York: Wiley) ch 7
[30] Goslar J, Hilczer W and Hoffmann S K 1998 *Inorg. Chem.* **37** 5936
[31] Williams F I B, Krupka D C and Breen D P 1974 *Phys. Rev.* **179** 255
[32] Hoffmann S K, Kaszyński R, Augustyniak M A and Hilczer W 1999 *Acta Phys. Polon.* A **96** 733